Materials and Design 36 (2012) 640–649

Contents lists available at SciVerse ScienceDirect

Materials and Design

journal homepage: www.elsevier.com/locate/matdes

Effect of heat treatment on ballistic impact behavior of Ti–6Al–4V against 7.62 mm deformable projectile

B. Bhav Singh *, G. Sukumar, Amit Bhattacharjee, K. Siva Kumar, T. Balakrishna Bhat, A.K. Gogia

Defence Metallurgical Research Laboratory, Kanchanbagh, Hyderabad 500 058, India

ARTICLE INFO

Article history:
Received 7 September 2011
Accepted 12 November 2011
Available online 25 November 2011

Keywords:
A. Ti–6Al–4V
C. Heat treatments
E. Impact and ballistic
A. Non-ferrous metals and alloys

ABSTRACT

The present study describes the effect of heat treatment on mechanical properties and ballistic impact resistance of Ti–6Al–4V alloy against 7.62 mm deformable lead projectiles. As-received plates were solution treated above and below the β-transus temperature followed by aging. The plates that were solution treated below the β-transus temperature followed by aging exhibited good combination of strength and ductility, and better ballistic impact resistance. Post ballistic microstructural examination showed formation of adiabatic shear bands (ASBs) and adiabatic shear band induced cracks. Both as-received plates and the plates that were solution treated above β-transus temperature followed by aging showed higher number of ASBs and ASB induced cracks compared to plates that were solution treated below β-transus temperature and then aged. Plug formation was observed through the ASB induced shear localization in planes parallel to the direction of projectile impact in all the conditions.

1. Introduction

Titanium alloys are being used in aerospace, chemical industries and in power plants due to their excellent combination of mechanical properties and corrosion resistance. Investigations have also been undertaken to examine the performance of these alloys in ballistic applications [1–10]. Although high strength polymers seem to have largely replaced the metallic materials in ballistic applications such as body armor and vehicle armor, materials such as Ti alloys hold promise because they have many advantages such as high specific strength, excellent multi-hit capability and easy formability. Traditionally, an α + β Ti alloy, Ti–6Al–4V has been used for various ballistic applications. Components made of Ti–6Al–4V have already been used in M2 Bradley fighting vehicle, M1A2 Abrams main battle tank and XM777 155 mm VSEL ultra lightweight Field Howitzer [1].

Since thermo-mechanical processing strongly influences microstructural and mechanical properties in titanium alloys, ballistic behavior may also be affected by thermo-mechanical processing. Burkins et al. [5] studied the effect of different thermo mechanical processing on the ballistic impact behavior of Ti–6Al–4V plates against 20 mm fragment simulating projectiles (FSPs) and 12.7 mm armor piercing (AP) projectiles. In that study, the plates that were either rolled or annealed above β-transus temperature showed a lower V_{50} ballistic limit in comparison to those that were α + β rolled or annealed. The magnitude of difference in V_{50} ballistic limit was found to be higher against FSP than against armor piercing projectiles. Bar and Rosenberg [6] analyzed the dynamic mechanical behavior and ballistic impact response of differently heat treated Ti–6Al–4V plates against 7.62 AP projectiles. It was found that β water quenched condition had better ballistic performance in comparison to as-received, β furnace cooled and α + β air cooled/water quenched conditions. In this study, the quasi-static strength and dynamic flow stress showed a direct correlation with ballistic performance. However other dynamic mechanical parameters such as failure strain (ε_f) or accumulated energy for failure ($\sigma \cdot \varepsilon_f$) did not show any correlation with ballistic performance.

Nemat-Nasser et al. [7] studied the dynamic response of conventional and hot isostatically pressed Ti–6Al–4V and found that ASB formation and associated fracture are the major failure mechanisms involved in Ti–6Al–4V at higher strain rates. It was observed in that study that initial microstructural features influence only the magnitude of threshold stress and athermal part of flow stress, but not the functional dependence of thermally activated part of flow stress on temperature and strain rate. Lee et al. [8,9] evaluated the effect of microstructural morphology such as Widmanstatten, equiaxed and bimodal, on dynamic deformation behavior of Ti–6Al–4V alloy using Split Hopkinson Pressure Bar (SHPB) and analyzed the energy spent in void nucleation and adiabatic shear band formation. It was found that bimodal microstructure exhibited higher resistance to adiabatic shear band (ASB) formation and higher V_{50} ballistic limit compared to other microstructures under dynamic conditions. In

* Corresponding author. Address: Armour Design and Development Division, Defence Metallurgical Research Laboratory, Kanchanbagh, Hyderabad 500 058, India. Tel.: +91 40 2458 6560/6355; fax: +91 40 2434 2252/0683.
E-mail addresses: bbsingh@dmrl.drdo.in, bhav_singh@rediffmail.com (B. Bhav Singh).

0261-3069/$ - see front matter © 2011 Elsevier Ltd. All rights reserved.
doi:10.1016/j.matdes.2011.11.030

another study [10], it was shown that the fine α_2 (Ti_3Al) formed in Ti–6Al–4V by over aging improves the quasi-static and dynamic mechanical properties and decreases ASB formation.

Even though many aspects of ballistic impact behavior of Ti–6Al–4V have been analyzed in the previous studies, most of the studies used non-deformable hard core projectiles such as 7.62 AP, 12.7 AP and fragment simulating projectiles (FSPs). The penetration mechanism involved in the 7.62 mm deformable projectile is different than that of non-deformable projectile [11,12]. The reported ballistic impact studies on Ti–6Al–4V alloy against 7.62 mm deformable ball projectiles are limited. Fanning [11] studied the effect of thickness on change in failure mode observed in Ti–6Al–4V against ball projectile. It was found that the predominant impact feature changed from formation and ejection of plug by ASB to bending and gross plastic deformation followed by fracture when the thickness was reduced. However, the role of microstructure on ballistic impact behavior of Ti–6Al–4V against soft core projectile such as 7.62 ball projectile has not been studied earlier. Such a study can facilitate better utilization of titanium alloys for applications against deformable projectiles such as body armor and vehicle armor. The present study is aimed at studying the ballistic impact behavior of Ti–6Al–4V with different microstructures against 7.62 mm deformable projectiles. Detailed post ballistic microstructural examination has been also carried out to understand the role of initial microstructures on deformation behavior under ballistic impact.

2. Material and experimental procedure

The Ti–6Al–4V alloy used in this study was received in the form of 15 mm thick plates in mill annealed condition from M/s. Mishra Dhatu Nigam Limited, Hyderabad, India. The β transus temperature of this alloy was found to be 985 °C ± 5 °C. These plates were subjected to different heat treatments i.e. solution treating above and below the β-transus temperature followed by aging as summarized in Table 1 to generate different microstructures. The 15 mm heat treated plates were machined to 12.7 mm and 10.0 mm thickness for ballistic trials. The room temperature mechanical properties were analyzed from the samples cut from the longitudinal direction of the 15 mm thick as-received and heat treated plates. The bulk hardness of as-received and heat treated plates were measured using Vickers hardness tester under a load of 30 kg. Room temperature tensile tests were carried out on cylindrical samples as per ASTM E8/8M-09 standard [13] at a strain rate of 8.3×10^{-4} using an Instron universal testing machine (Instron 5500R). For each condition, five samples were tested and average values are reported in this paper.

The ballistic tests were carried out on as-received and heat treated plates of 300 mm × 300 mm × t (t = 15 mm, 12.7 mm and 10 mm) against 7.62 mm deformable projectiles in order to find whether a plate is able to stop the projectile at a given thickness or not. The target plates were impacted at 0° angle of attack using a standard rifle in a small arms range. The gun was mounted on a rigid mount with holding devices and properly aligned on a level plane. The ballistic testing arrangement is given in Fig. 1a. The projectile was fired from a distance of 10 m with a striking velocity of 830 ± 10 m/s. The impact velocity of the projectile was measured in each test with the help of instrumented velocity measuring equipment. Three plates for each heat treatment were evaluated for ballistic performance and each target plate was subjected to five shots. In order to prevent any overlap between any two shots, distance between two impact craters on the plate was maintained more than three times the diameter of the projectile. The distance between the edges to any shot has also been maintained at least three times the diameter of the projectile based on the guidelines given by MIL-A-46100D standard [14]. Fig. 1b presents a general and cross section view of the projectile with its core. The projectile had antimony alloyed lead core with a surrounding brass jacket. The hardness of the lead core was 12 VHN. The projectile had a diameter of 7.62 mm and length of 28.5 mm. The nominal mass of the projectile was 9.03 g with brass jacket and 6.05 g without the brass jacket.

After ballistic trials, the damage patterns in the front and back face of target plates were photographed to describe the failure mechanism involved in penetration of different heat treated plates. The microstructures of the initial heat treated samples and post ballistic impact cross sections were analyzed using standard optical metallographic technique and scanning electron microscopy.

3. Results and discussion

3.1. Microstructure and mechanical properties

Fig. 2 shows the scanning electron micrographs of as-received and different heat treated target plates. The as-received sample shows a microstructure consisting almost of equiaxed primary α and small amounts of retained β. The β solution treated and aged (1000 °C STA) sample has a microstructure consisting of acicular martensite (α′) within prior beta grains. The prior beta grain size is about 490 μm. The α + β solution treated and aged (950 °C STA and 900 °C STA) samples have bimodal structure with different volume fractions of equiaxed primary α and transformed β. The volume fraction of primary α phase in 950 °C STA and 900 °C STA conditions is about 21% and 40% respectively.

Fig. 3 shows the engineering tensile stress–strain curves of alloy in different conditions. The various tensile test parameters such as yield strength, ultimate tensile strength, %elongation, area under stress–strain curve, and hardness values are summarized in Table 2. It is clear from the Fig. 3 and Table 2 that the as-received condition has lowest yield strength and ultimate tensile strength (UTS) with a ductility of 9.0%. The 1000 °C STA condition with acicular transformed β microstructure has a slightly higher yield strength and tensile strength compared to as-received condition, but with lower %elongation of 4.5%. The 950 °C STA and 900 °C STA conditions with bimodal microstructures have higher ultimate tensile strength together with good ductility. This higher strength and ductility of bimodal microstructures in comparison to fully transformed β microstructure has been attributed to their shorter effective slip length [15]. The 950 °C STA and 900 °C STA conditions also have higher area under the engineering stress–strain curve compared to as-received and 1000 °C STA conditions. The quasi-static mechanical property trends observed in the present study are in

Table 1
Heat treatment conditions used in the present study and their designations.

Material	Heat treatment	Designation	Microstructure
Ti–6Al–4V	Mill annealed	As received	Equiaxed
	1000 °C/1 h/water quenching + 540 °C/4 h/air cooling	1000 °C STA	Acicular
	950 °C/1 h/water quenching + 540 °C/4 h/air cooling	950 °C STA	Bimodal
	900 °C/1 h/water quenching + 540 °C/4 h/air cooling	900 °C STA	Bimodal

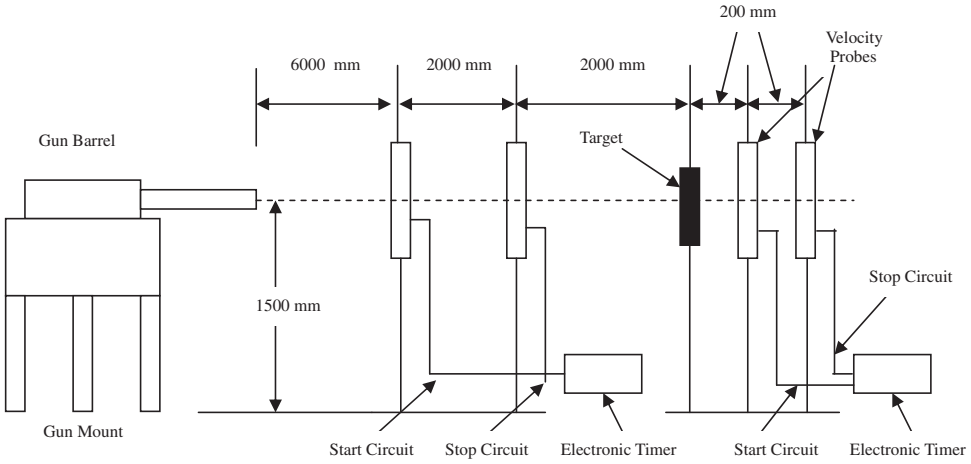

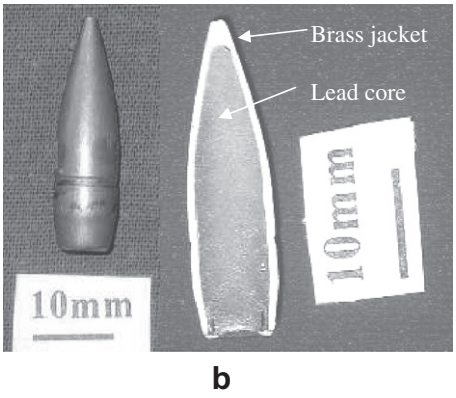

Fig. 1. (a) Schematic diagram of the ballistic test arrangement (b) general and cross sectional view of 7.62 mm projectile with copper jacket and lead core.

agreement with the previous results [8,9,15]. The high strain rate deformation behavior of microstructural conditions investigated in the present study has also been reported in the literature [8,9]. It suggests that bimodal microstructures which show higher energy absorption at quasi-static strain rates also have better energy absorption at higher strain rates in comparison to equiaxed and widmanstatten microstructures.

3.2. Ballistic impact studies

Table 3 summarizes the ballistic test results of all the conditions at different thicknesses. At 15 mm thickness, all the plates are able to stop the projectile without perforation. Fig. 4a–d shows the front face of the 15 mm thick as-received and different heat treated plates after the ballistic impact. It is clear that the impact crater formed in the as-received condition (Fig. 4a) is wider and deeper compared to other conditions. The solution treated and aged conditions have narrow craters with smaller depth possibly due to their higher yield and ultimate tensile strength. Fig. 4e–h shows the rear faces of the as-received and different heat treated plates. The as-received condition (Fig. 4e) has smooth bulge on the rear face. The 1000 °C STA condition (Fig. 4f) does not show any bulge, but it contains radial cracks. This could be attributed to the poor ductility of 1000 °C STA condition. The rear faces of 950 °C STA and 900 °C STA conditions (Fig. 4g and h) are very smooth without any bulge or cracks. The plates in 950 °C STA and 900 °C STA conditions have higher tensile strength and good ductility and they are able to absorb the projectile's kinetic energy more effectively.

Fig 5a–d shows the front face and rear face along with penetration channel of the 12.7 mm as-received and heat treated plates after the ballistic testing. The projectile has perforated the 12.7 mm thick plates in as-received (Fig. 5a) and 1000 °C STA conditions (Fig. 5b). Even though the projectile has penetrated completely through the thickness of both as-received and 1000 °C STA condition, the failure modes associated with two plates are different. The front face of the as-received condition (Fig. 5a) has a small front spall around the periphery of the penetration channel. The rear face of the as-received condition shows a spall ring and petals indicating that plug has formed after the bulging. The 1000 °C STA condition (Fig. 5b) has a small front spall region followed by smooth plug region without any petals at rear face. Comparison of present observations with previous studies [11,12,16,17] suggests that the perforation in as-received condition is a result of spalling, plug formation by ASB induced shear localization and petaling. However in case of 1000 °C STA the perforation involves only front spalling and plug formation through ASB induced shear localization. The 12.7 mm thick plates that are solution treated below the beta transus temperature and aged are able to stop the projectile without perforation. Fig. 5c and d shows smooth surface and smooth bulge observed in the rear faces of the 12.7 mm thick plates in 950 °C STA condition and 900 °C STA condition respectively. Since the plug has already formed in 12.7 mm plates of as-received and 1000 °C STA condition, lower thickness plates were not tested further for these conditions. The lower thickness (10 mm) trials of 950 °C STA and 900 °C STA plates were carried out to understand the failure mode involved in the perforation.

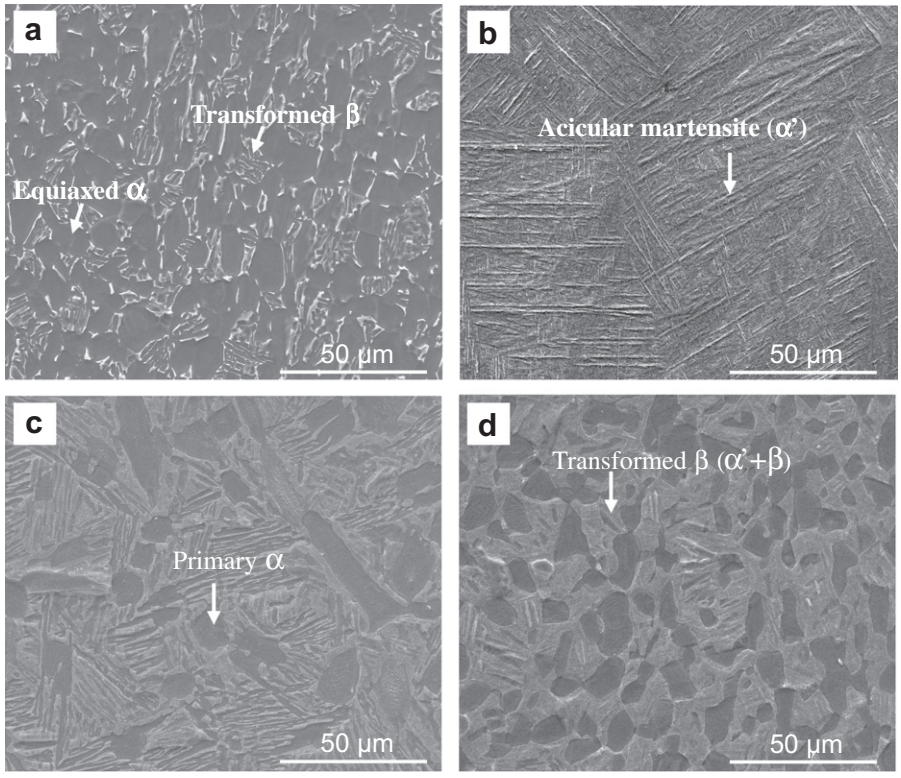

Fig. 2. Scanning electron micrographs of Ti–6Al–4V plates at different conditions (a) as-received (b) 1000 °C STA (c) 950 °C STA (d) 900 °C STA.

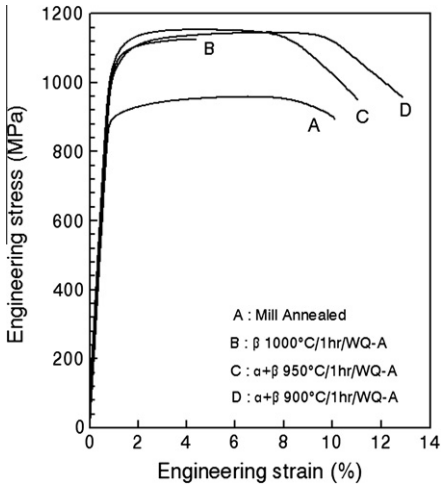

Fig. 3. Engineering stress–strain curves of Ti–6Al–4V alloy at different conditions.

Projectile is able to completely pass through 10 mm plates in 950 °C STA and 900 °C STA conditions. Fig. 6a and b shows the front face, rear face and penetration channel formed in the 10 mm thick plates in 950 °C STA and 900 °C STA conditions. In both the plates, front face contains small front spall and the rear face contains petals. Thus the damage patterns associated with perforation in these two conditions also contain front spall, plug formation by ASB induced shear localization and petaling. Penetration channel diameters observed in all conditions are higher than original projectile diameter. This is because projectile undergoes large deformations and gets flattened before the formation of plug.

When the deformable projectile strikes the target plate, part of its kinetic energy is consumed in deforming the projectile itself and the remaining part of the energy is imparted to the target material [12,18]. The main mechanism by which the ductile target material absorbs the projectile's kinetic energy is by plastic flow [16,19,20].

Table 3
Ballistic test results of the different conditions.

Condition	Thickness(mm)	Perforation (Yes/No)	Rear face observation
As received	15.0	No	Smooth bulge
	12.7	Yes	Petaling
1000 °C STA	15.0	No	Radial cracks
	12.7	Yes	No Petaling
950 °C STA	15.0	No	Smooth surface
	12.7	No	Smooth surface
	10.0	Yes	Petaling
900 °C STA	15.0	No	Smooth surface
	12.7	No	Smooth bulge
	10.0	Yes	Petaling

Table 2
Mechanical properties of the Ti–6Al–4V alloy at different conditions.

Condition	0.2% YS (MPa)	UTS (MPa)	Elongation to failure (%)	Area under engineering stress–strain curve (MJ/m^3)	Hardness (VHN)
As received	906 ± 5	961 ± 7	9.0 ± 1.0	92	285
1000 °C STA	1036 ± 18	1112 ± 20	4.5 ± 0.3	44	376
950 °C STA	1050 ± 20	1143 ± 11	10.7 ± 0.5	120	335
900 °C STA	1018 ± 17	1123 ± 12	12.7 ± 1.0	137	332

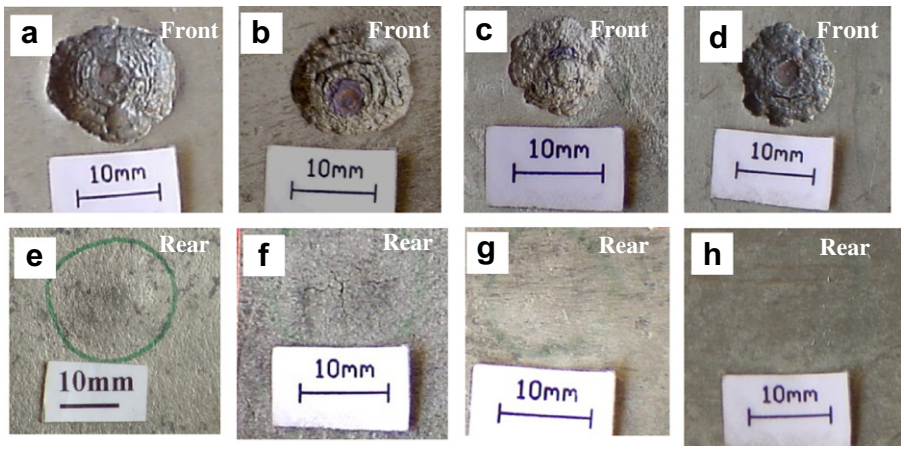

Fig. 4. Front and rear faces of the impact areas of 15 mm thick plates (a and e) as-received condition (b and f) 1000 °C STA condition (c and g) 950 °C STA condition (d and h) 900 °C STA condition.

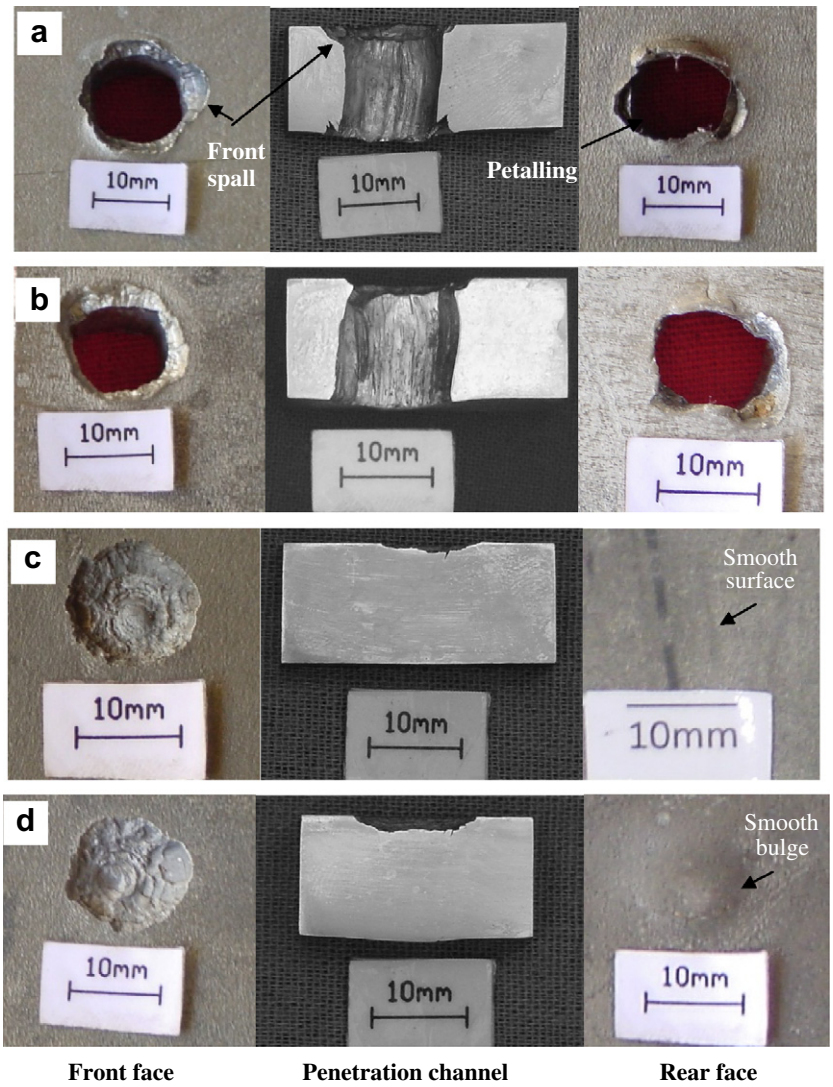

Fig. 5. Front and rear face along with the impact penetration channel of 12.7 mm thick plates (a) as-received (b) 1000 °C STA (c) 950 °C STA (d) 900 °C STA.

Higher the strength of a material more is the energy required for its plastic flow. Recent study by Borvik et al. [21] on ballistic impact behavior of five different steel grades against 7.62 mm ball projectile has shown that as the yield strength increases the perforation resistance increases. It has been pointed out that the material strength is an important factor than ductility for the protection against small arms projectiles. In that study, the plastic work per unit volume calculated from area under the true stress–strain

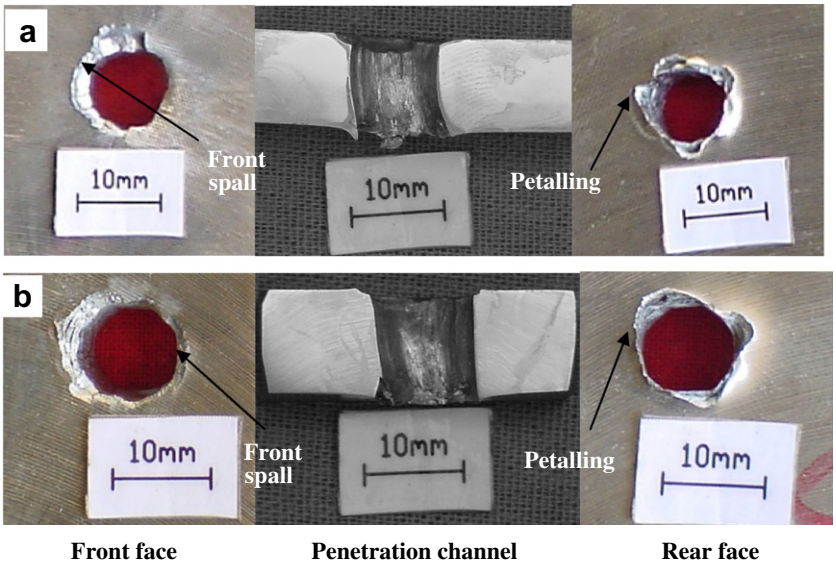

Fig. 6. Front and rear face along with the impact penetration channel of 10 mm thick plates (a) 950 °C STA condition (b) 900 °C STA condition.

curve also did not correlate with the perforation resistance. The present study however indicates that both strength and ductility play a role in imparting ballistic resistance. Thus, 950 °C STA and 900 °C STA conditions which have good combination of strength and %elongation are able to stop the projectile at 12.7 mm thickness. Both the as-received plate having lower strength with good %elongation and 1000 °C STA plates having higher strength with lower %elongation have been perforated at 12.7 mm thickness. Qualitatively, it can be stated that higher area under the stress–strain curve (which is determined both by strength and ductility) leads to improved ballistic resistance. It has to be noted that correlating ballistic performance with static mechanical properties is only an empirical method, which helps in screening potential microstructural conditions for armor applications. Better correlation may be found with high strain rate mechanical properties, since actual ballistic impact event involves higher strain rates. Comparison of present ballistic results with previous high strain rate mechanical data [8,9] indicates that the better ballistic performance of 950 °C STA and 900 °C STA conditions with bimodal microstructures could be due to their better energy absorption at higher strain rates in comparison to as-received (equiaxed microstructure) and 1000 °C STA (acicular microstructure).

In order to better understand the role of mechanical properties and microstructures on the perforation resistance, detailed post ballistic microstructural analysis of 15 mm impact crater cross sections has been carried out. Since, the perforation of the Ti–6Al–4V target plates against ball projectile has been found to involve ASB induced plugging when thickness of the target plate is higher than the projectile diameter [11], specific attention has been directed on observation of the adiabatic shear bands and ASB induced cracks. Figs. 7 and 8 show the optical microstructures of impact crater cross section in 15 mm thick as-received and various heat treated plates. The optical microstructure of the crater cross section in as-received plate is shown in Fig. 7a. It may be observed that a number of adiabatic shear bands emanate from the crater wall. In certain locations, ASB induced cracks are also seen along the path of ASBs. Pictures of two prominent ASBs with ASB induced cracks observed in the locations marked A and B are enlarged in Fig. 7b and c. The 1000 °C STA condition also has higher number of ASBs. Two long ASB induced cracks were observed at two locations at the end of the crater as shown in Fig. 8a. The 950 °C STA and 900 °C STA conditions have less number of ASBs compared to as-received and 1000 °C STA conditions. The ASB induced crack is not observed in 950 °C STA crater cross section (Fig. 8b) and only one ASB induced crack is observed in 900 °C STA crater cross section, Fig. 8c.

During ballistic impact, high strains develop at the impact location of the target material within a short period. Hence, the process of heating by conversion of plastic work in short period of time can be considered as adiabatic. Such conditions can generate adiabatic shear bands. In the case of penetration by projectiles, these are highly strained narrow annulus regions, only a few microns wide and formed in certain locations. They form when the combined effects of strain-hardening and strain rate hardening of the material is overwhelmed by the thermal softening resulting from heat evolved from plastic deformation [22]. Recent study by Rittel and Wang [23] on thermo-mechanical aspects of ASB failure in Ti–6Al–4V has shown that thermal softening is indeed influential in ASB formation in Ti–6Al–4V. In another study [24], it was pointed out that ASB failure is not only a mechanical instability, but also a result of microstructural rearrangements leading to localized material softening prior to any thermal softening. It was also shown that dynamic recrystallization observed inside ASB is not a consequence of high local temperature and strains, instead it precedes and triggers the ASB failure [24]. The formation of ASB has been analyzed using various material parameters such as strain hardening coefficient, density, specific heat, strain rate sensitivity, flow stress and strains [25,26]. It is well known that the titanium alloys are prone to adiabatic shear banding due to their high sensitivity of flow stress to temperature, low strain hardening rate and poor thermal conductivity [25,26].

Table 4 summarizes the various post-ballistic microstructural observations such as number of ASB nucleating points and ASB induced cracks, variation in ASB width and average width of ASB in impact craters of 15 mm thick targets. In the present study the number of white etching ASBs are found to be higher in as-received and 1000 °C STA conditions compared to 950 °C STA and 900 °C STA conditions. This observation matches well with the previous dynamic deformation studies. Previous dynamic deformation studies [8,9,27] have reported that bimodal microstructures have higher energy absorption and greater resistance to ASB formation compared to equiaxed and lamellar microstructures at high strain rates. It has been shown that as the effective grain size measured in terms of colony size or α lamellar spacing increases the possibility of adiabatic shear band formation increases [28]. The $\alpha + \beta$ solution

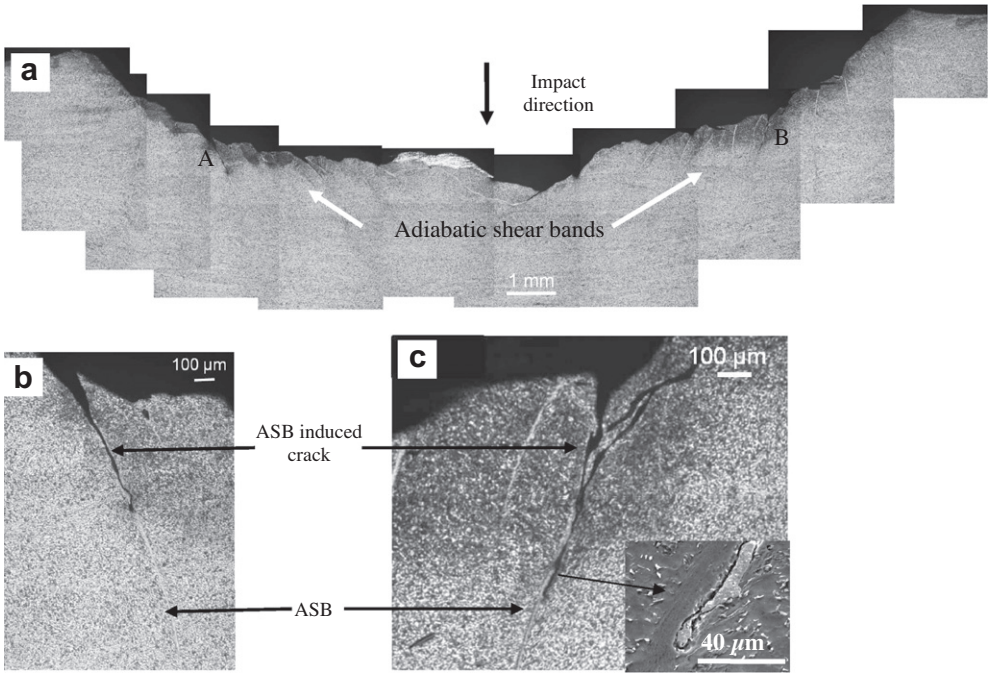

Fig. 7. (a) Optical microstructure of the impact crater cross section in 15 mm thick as- received condition (b) enlarged view of the ASB induced cracks formed along ASB at location A and (c) location B (SEM image of ASB induced crack is embedded in the bottom).

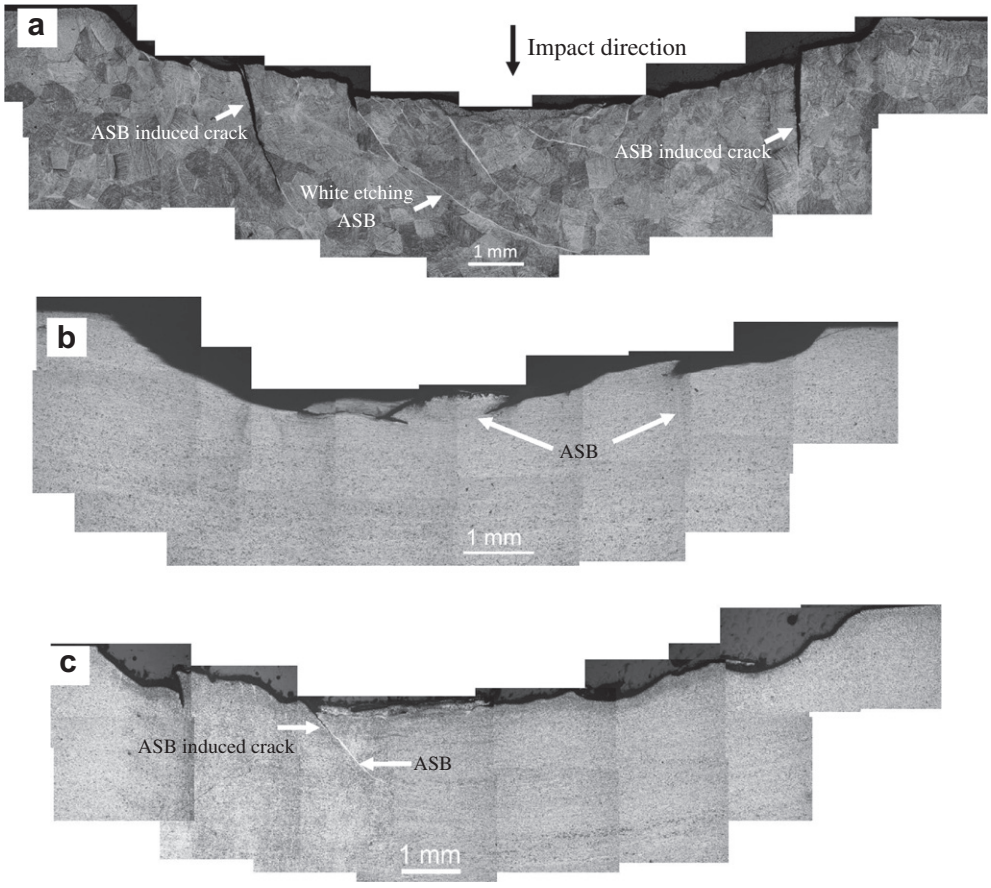

Fig. 8. Optical microstructure of the impact crater cross section in 15 mm thick plates of (a) 1000 °C STA condition (b) 950 °C STA condition (c) 900 °C STA condition.

treated bimodal microstructures have finer grain size compared to β solution treated, fully transformed β microstructure. Hence, the formation of adiabatic shear band is greatly reduced.

The width of white etching ASBs corresponding to different conditions vary from 3 to 50 μm. The ASB width observed in the present study matches well with the results previous investigations

Table 4
Post ballistic observations on the impact crater optical microstructures of 15 mm thick plates.

Condition	No of ASB nucleating points	No of ASB induced crack	ASB width variation (μm)	Average width of ASB (μm)	Length of ASB induced crack (μm)
As received	20	5	3–45	12 ± 6	732,647*
1000 °C STA	19	2	4–50	18 ± 8	1840,2300
950 °C STA	2	–	3–13	8.0 ± 3	–
900 °C STA	6	1	4–42	15 ± 8	510

* Refers length of the prominent ASB induced cracks measured at locations marked A and B in Fig. 7a.

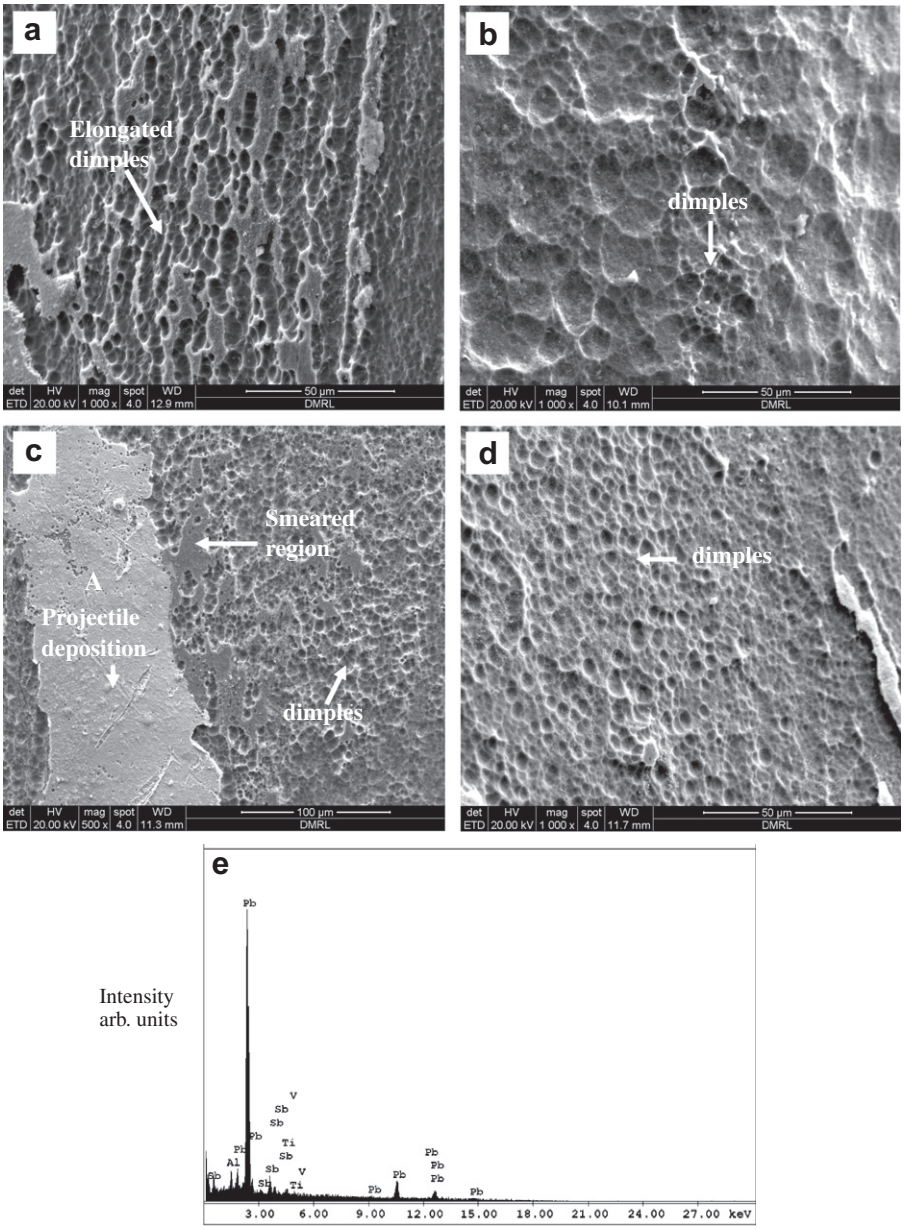

Fig. 9. SEM image of fracture surface at penetration channel midsection of (a) 12.7 mm thick as-received condition (b) 12.7 mm thick 1000 °C STA condition (c) 10 mm thick 950 °C STA condition (d) 10 mm thick 900 °C STA condition (e) EDAX showing deposition of projectile material on the crater wall in location A in figure (c).

[27–31]. According to Dodd and Bai [32], the width of ASB mainly depends on the strain rate and thermal properties of the material and it does not depend on the details of imposed combined stress state. Various analytical solutions for ASB width [32–34] have predicted that as the local strain rate increases, the width of the ASB comes down. In case of a ballistic impact event, the strain rate developed in a particular region is a function of its distance from the point of impact. Hence, a range of ASB width is observed in the crater microstructure depending on the range of strain rates developed at different regions during a given impact. It has been observed in the previous studies on aluminum alloys [35,36] and steels [37] that as the strength of the target material increases, the width of the ASB come down. However, in the present study, it has not been possible to observe such a correlation. The differ-

ence in average ASB width between different conditions is also not very large.

Apart from ASBs, few ASB induced cracks are also seen around the crater cross section. Due to the higher cooling rate experienced by the material inside the ASB, the microstructure of the ASB is different from the parent microstructure [29]. Due to the large temperature rise and higher strains associated with the ASBs, void formation and their link up is preferentially promoted within the regions of ASB [29,38]. Cracks are easily formed in these regions under the action of tensile stress acting perpendicular to the shear surfaces [29,38]. In the present study, higher numbers of ASB induced cracks are observed in the craters of as-received and 1000 °C STA condition. The prominent through thickness ASB induced cracks have propagated higher distance in as-received and 1000 °C STA plates than the plates of 950 °C STA and 900 °C STA conditions (Table 4). These prominent ASB induced cracks assist plug formation by linking to the rear face. These observations suggest that as-received and 1000 °C STA conditions are prone to easier plug formation by ASB induced shear localization. Thus these plates fail at 12.7 mm thickness itself Fig. 5a and b. However, in the case of 950 °C STA condition, no ASB induced crack is observed. The 900 °C STA condition has only one ASB induced crack and it has travelled less distance in thickness direction of the plate. This indicates that plug formation by ASB induced shear localization in these microstructures is more difficult. As a result, even at 12.7 mm thickness level, these target plates are able to stop the projectile without perforation Fig. 5c and d. The projectile is able to form plug in these heat treated conditions in 10 mm thick plates.

To clarify the role of ASB in plug formation, Fig. 9a–d shows the SEM fractographs taken at the midsection of the penetration channels. The penetration channel surfaces exhibit two type of fracture characteristics, namely ductile dimples and smeared regions as reported in the previous studies [8,27,39,40]. The ductile dimples are known to be formed due to the tensile stresses within the adiabatic shear bands. The microvoids nucleate, grow and coalesce within the adiabatic shear bands under the action of tensile stresses which results in dimple formation followed by fracture. The smeared regions are suggested to be formed by the rubbing of adjoining hot fractured surfaces [8,27,39,40]. In some locations, the deposition of projectile material on the fracture surface has also been observed (Fig. 9e). Hence it is clear that irrespective of the difference in initial microstructures and mechanical properties, the plug formation in Ti–6Al–4V plates against 7.62 mm deformable projectile is through the ASBs along projectile–target interface.

Burkins et al. [5] observed in their ballistic study of different heat treated Ti–6Al–4V plates against 20 mm FSP that plug formation is by ASB induced shear localization. In the present study against 7.62 mm deformable projectile also, the plug formation involves ASB induced shear localization irrespective of the initial microstructures. It is clear from the present study that for attaining higher ballistic performance against 7.62 mm deformable projectiles higher energy absorption at higher strain rates and higher resistance to adiabatic shear banding is needed.

4. Conclusions

The plates that are solution treated below β-transus temperature and then aged have a higher ballistic impact resistance compared to both as-received and β solution treated and aged plates due to higher energy absorption at higher strain rates and greater resistance to adiabatic shear localization. The number of adiabatic shear bands and adiabatic shear band induced cracks are higher in as-received and β solution treated and aged plates compared to plates that are solution treated below the β-transus and then aged. Plug formation in all conditions is associated with ASB induced shear localization occurring parallel to the direction of the projectile impact.

Acknowledgements

The authors wish to express their gratitude to the Director, DMRL for granting permission to publish this paper. The authors would like to thank DRDO for funding this work. The authors wish to thank Small Arms Range team of DMRL for their help in carrying out ballistic trials.

References

[1] Montgomery JS. Low-cost titanium armors for combat vehicles. JOM 2001;49(5):29–32.
[2] Bruchey WJ. Suppression of material failure modes in titanium armors. Army research laboratory, ARL-TR-3124; 2003. p. 1–24.
[3] Bless J, Gooch W, Sathapathy S, Campos J, Lee M. Penetration resistance of titanium and ultra-hard steel. Int J Impact Eng 1997;20:121–9.
[4] Walters W, Gooch W, Burkins MS. The penetration resistance of a titanium alloy against jets from tantalum shaped charge liners. Combust Explos Shock Waves 2000;36(6):745–50.
[5] Burkins MS, Hansen JS, Paige JI, Turner PC. The effect of thermomechanical processing on the ballistic limit velocity of extra low interstitial titanium alloy Ti–6Al–4V. Army research laboratory, ARL-MR-486, 2000. p. 1–69.
[6] Bar YM, Rosenberg Z. On the correlation between the ballistic behavior and dynamic properties of titanium-alloy plates. Int J Impact Eng 1997;19(4):311–8.
[7] Nemat-Nasser S, Guo WG, Nesterenko VF, Indrakanti SS, Gu YB. Dynamic response of conventional and hot isostatically pressed Ti–6Al–4V alloys: experiments and modeling. Mech Mater 2001;33:425–39.
[8] Lee DG, Kim S, Lee S, Lee CS. Effects of microstructural morphology on quasi-static and dynamic deformation behavior of Ti–6Al–4V. Metall Trans A 2001;32A:315–24.
[9] Lee DG, Lee YH, Lee S, Lee CS, Hur S. Dynamic deformation behavior and ballistic impact properties of Ti–6Al–4V alloy having equiaxed and bimodal microstructures. Metall Trans A 2004;35A:3103–12.
[10] Lee DG, Kim YG, Nam DH, Hur SM, Lee S. Dynamic deformation behavior and ballistic performance of Ti–6Al–4V alloy containing fine α_2 (Ti_3Al) precipitates. Mater Sci Eng A 2005;391:221–34.
[11] Fanning JC. Ballistic Evaluation of Ti–6Al–4V plate for protection against small arms projectiles. In: Lutjering G, Albrecht J, editors. Proceedings of the 10th world conference on Titanium (Ti-2003 Science and Technology), Hamburg, Germany; 2003, p. 3125–31.
[12] Jena PK, Mishra B, Siva Kumar K, Bhat TB. An experimental study on the ballistic impact behavior of some metallic armour materials against 7.62 mm deformable projectile. Mater Design 2010;31(7):3308–16.
[13] ASTM E8/8M-09. Standard test methods for tension testing of metallic materials. American Society for Testing and Materials, Annual book of ASTM Standards; 2009.
[14] MIL-A-46100D standard. Military specification for ballistic testing of armor plate, steel, wrought high hardness; 1988. p. 1–27.
[15] Lutjering G. Influence of processing on microstructure and mechanical properties of ($\alpha + \beta$) titanium alloys. Mater Sci Eng A 1998;243:32–45.
[16] Backman ME, Goldsmith W. The mechanics of penetration of projectile into targets. Int J Eng Sci 1978;16:1–99.
[17] Woodward RL. The interrelation of failure modes observed in the penetration of metallic targets. Int J Impact Eng 1984;2(2):121–9.
[18] Papukutty KK, Madhu V, Ramanjaneyulu K, Bhat TB.In: Proceedings of the 8th international symposium on plasticity and impact (IMPLAST 2003), New Delhi; 2003, p. 190.
[19] Srivathsa B, Ramakrishnan N. Ballistic performance for thick metallic armour. J Mater Process Technol 1999;96:81–91.
[20] Bhat TB. Principles of armour design. Trans Indian Inst Met 1984;37:313–35.
[21] Borvik T, Dey S, Clausen AH. Perforation resistance of five different high-strength steel plates subjected to small-arms projectiles. Int J Impact Eng 2009;36:948–64.
[22] Woodward RL. Metallographic features associated with the penetration of titanium alloy targets. Metall Trans A 1979;10A:569–73.
[23] Rittel D, Wang ZG. Thermo-mechanical aspects of adiabatic shear failure of AM50 and Ti6Al4V alloys. Mech Mater 2008;40:629–35.
[24] Rittel D, Landau P, Venkert A. Dynamic recrystallization as a potential cause for adiabatic shear failure. Phys Rev Lett 2008;101:165501–4.
[25] Timothy SP. The structure of adiabatic shear bands in metals: a critical review. Acta Metall 1987;35(2):301–6.
[26] Shahan AR, Karimi Taheri A. Adiabatic shear bands in titanium and titanium alloys: a critical review. Mater Design 1993;14(4):243–50.
[27] Liu X, Tan C, Zhang J, Wang F, Cai H. Correlation of adiabatic shearing behavior with fracture in Ti–6Al–4V alloys with different microstructures. Int J Impact Eng 2009;36:1143–9.
[28] Lee DG, Lee S, Lee CS, Hur S. Effects of microstructural factors on quasi-static and dynamic deformation behaviors of Ti–6Al–4V alloys with widmanstätten structures. Metall Trans A 2003;34A:2541–54.

[29] Bar YM, Shechtman D. On the adiabatic shear of Ti–6A1–4V ballistic targets. Mater Sci Eng A 1983;58:181–8.
[30] Liao SC, Duffey J. Adiabatic shear bands in Ti–6Al–4V titanium alloy. J Mech Phys Solids 1998;46(11):2201–31.
[31] Grebe HA, Pak H, Meyers MA. Adiabatic shear localization in titanium and Ti–6 pct Al–4 pct V alloy. Metall Trans A 1985;16:761–75.
[32] Dodd B, Bai Y. Width of adiabatic shear bands formed under combined stresses. Mater Sci Technol 1989;5:557–9.
[33] Grady DE, Kipp ME. The growth of unstable thermoplastic shear with applications to steady wave shock compression in solids. J Mech Phys Solids 1987;32:95–118.
[34] Wright TW, Ockendon H. A model for fully formed shear bands. J Mech Phys Solids 1992;40:1217–26.
[35] Lee CG, Lee S. Correlation of dynamic torsional properties with adiabatic shear banding behavior in ballistically impacted aluminum–lithium alloys. Metall Trans A 1998;29A:227–35.
[36] Leech PW. Observations of adiabatic shear band formation in 7039 aluminum alloy. Metall Trans A 1985;16(10):1900–3.
[37] Solberg JK, Leinum JR, Embury JD, Dey S, Børvik T, Hopperstad OS. Localised shear banding in Weldox steel plates impacted by projectiles. Mech Mater 2007;39:865–80.
[38] Xu Y, Bai Y, Meyers MA. Deformation, phase transformation and recrystallization in the shear bands induced by high-strain rate loading in titanium and its alloys. J Mater Sci Technol 2006;22(6):737–46.
[39] Liu X, Tan C, Zhang J, Hu Y, Ma H, Wang F, et al. Influence of microstructure and strain rate on adiabatic shearing behavior in Ti–6Al–4V alloys. Mater Sci Eng A 2009;501:30–6.
[40] Timothy SP, Hutchings IM. Initiation and growth of microfractures along adiabatic shear bands in Ti–6Al–4V. Mater Sci Technol 1985;1:526–30.